A Side-Loaded-Metal Decoupling Method for 2×N Patch Antenna Arrays

Zhang, Yiming; Zhang, Shuai

Published in:
I E E E Antennas and Wireless Propagation Letters

DOI (link to publication from Publisher):
10.1109/LAWP.2021.3059736

Publication date:
2021

Document Version
Accepted author manuscript, peer reviewed version

A Side-Loaded-Metal Decoupling Method for 2×*N* Patch Antenna Arrays

Yi-Ming Zhang, *Member, IEEE*, and Shuai Zhang, *Senior Member, IEEE*

***Abstract*—To suppress the strong mutual coupling among 2×*N* patch antenna arrays, a very simple decoupling method is presented in this article, where only a metal block is utilized and loaded in the center of the 2×*N* arrays. With the proposed method, the coupling between horizontal, vertical as well as diagonal pairs of adjacent antenna elements are well suppressed to a low level. To verify the practical performance, a 2×8 antenna array centered at 3.5 GHz and integrated with the proposed decoupling method is further developed and fabricated. The measured results denote that the maximum mutual coupling among the array is suppressed from −15.4 dB to −26.9 dB, with a fairly low insertion loss level. The design and implementation of the proposed decoupling method are very simple with a low profile and can be widely used for large-scale array applications with the 2×*N* configuration.**

***Index Terms*—Multiple-input multiple-output (MIMO), massive MIMO, patch antenna decoupling, metal block.**

I. Introduction

As a promising technology for the fifth generation and beyond wireless communication applications, massive multiple-input multiple-output (MIMO) system is attracting increasing attention since it enables continuously exchanging of a huge number of audio, video as well as the coming holographic for every covered user equipment [1], [2]. The massive MIMO antenna array, a kind of large-scale antenna array, is one of the essential and key components of the massive MIMO systems. In general, massive MIMO antenna arrays are designed with small inter-element distances for wide-angle steering purposes. However, the active impedance matching of antennas would suffer from the strong mutual coupling among the antennas due to the small inter-element distance, with some other negative effects [3], [4]. To reduce the coupling effect and achieve wide steering-angle purposes, additional decoupling approaches are normally essential [5]-[20]. According to the published investigations, in massive MIMO antenna arrays, the coupling level should be suppressed to less than −25 dB, from the active impedance matching performance and linearity of the power amplifies point of view [3], [15], [18], [19].

For small-scale antenna arrays, many efforts have been devoted to reducing the coupling such as decoupling networks [5], electromagnetic band-gap structure [6], decoupling resonator [7], dummy-element-based method [8], decoupling metasurface [9], defected ground [10], scatter-loaded scheme [11], and self-decoupled antennas [12], [13]. As for large-scale arrays, the decoupling would be more challenging since the mutual coupling is much more complicated compared to the two- or three-element arrays [14]-[20]. In [15] and [16], decoupling surfaces were studied for *M*×*N* antenna arrays, at the cost of bulky size since the decoupling surfaces were approximately a quarter-wavelength away from the antenna aperture. The network-based decoupling method is also an alternative for large-scale arrays [17], [18]. For instance, a lattice-shaped decoupling network was studied for *M*×*N* patch antenna arrays in [18]. With the approach, the mutual coupling among all the elements are well-suppressed at the center frequency, but featuring a narrow decoupling bandwidth owing to the strong decoupling resonance. The above approaches are complicated since specified decoupling structures or tedious mathematical derivations are generally required. More recently, some decoupling methods with simple configurations or design procedures were presented [19], [20]. In [19], a wavetrap-based decoupling method was proposed for 45°-polarized patch arrays, with about 10%-14% degradation in total efficiency.

In this letter, a very simple decoupling method is proposed for 2×*N* patch antenna arrays consisting of two linear subarrays. By loading a metal block in between the two subarrays, the E-plane coupling, H-plane coupling, and diagonal coupling are all suppressed. Notice that inserting a metal block in between patch antennas to improve the isolation is reported which is only effective for the configuration where the antennas should be positioned on the two sides of the metal block, reflecting a one-dimensional decoupling function. As for the proposed scheme in this letter, the antennas positioned on either the two sides or the same side of the block are all decoupled, achieving a two-dimensional decoupling by using a single metal block. The loss introduced by the metal block is fairly small, making the approach to be attractive for massive MIMO systems.

II. Analysis of Proposed Decoupling Method

Here, a 2×8 patch antenna array centered at 3.5 GHz is chosen as the study case. Shown in Fig. 1 is the configuration of the array integrated with the proposed side-loaded reflector for decoupling purposes. The center distance between the adjacent elements, i.e. *Wd*, is 42.8 mm, representing a half-wavelength distance. Notice that the stacked-substrate configuration is employed to achieve a wide impedance bandwidth, which has no contribution to the proposed decoupling method. The mutual

This work was supported by Huawei project of "5G mmWave Decoupling Array". (*Corresponding author*: *Shuai Zhang*.)

The authors are with the Antenna, Propagation and Millimeter-wave Systems (APMS) Section, Aalborg University, 9220 Aalborg, Denmark (e-mail: yiming@es.aau.dk; sz@es.aau.dk).

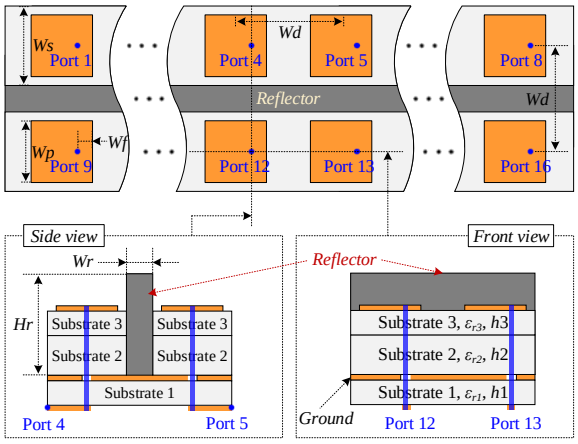

Fig. 1. Configuration of the 2×8 patch array with the proposed decoupling method, where Wp = 24 mm, Wf = 4.8 mm, Ws = 37.8 mm, Wd = 42.8 mm, Wr = 5 mm, Hr = 14 mm, $h1$ = 0.762 mm, $h2$ = 4 mm, $h3$ = 0.254 mm, ε_{r1} = 3.66, ε_{r2} = 2.2, ε_{r3} = 3.66.

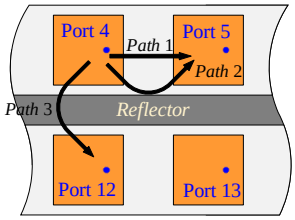

Fig. 2. Diagram of the mutual coupling paths of Port 4.

coupling among the array can be well-suppressed by utilizing the simple metal block positioned between the two eight-element subarrays, as illustrated in Fig. 1. Particularly, both the vertical and horizontal pairs of adjacent antenna elements are decoupled. Here, port 4 is selected as the representative port to describe the decoupling method, as plotted in Fig. 2. From port 4 to port 5, there are two leaking paths, the direct coupling path 1 and the reflecting path 2. Path 3 describes the main coupling between port 4 and port 12. By designing the metal block with proper height Hr and width Wr, path 1 and path 2 will be canceled with each other at the interface of port 5, and the magnitude of path 3 will be significantly reduced, leading to a high decoupling level. As for the mutual coupling between diagonal or non-adjacent pairs of antenna elements, it is rather to do nothing than employ additional decoupling structure, since the mentioned coupling is already with a very small magnitude generally.

Parameter investigations are further carried out to give a visible design guideline of the decoupled array, as depicted in Fig. 3 where the coupling $S_{5,4}$ and $S_{12,4}$ with different sizes of the metal block are given. It is found that with a height of higher than 3 mm, the horizontal coupling $S_{5,4}$ would be less than −25 dB. Moreover, a decoupling resonance would be generated close to the center frequency, when the height increases to 11 mm, as shown in Fig. 3(a). Seeing that the distance between the elements and the block is fixed when the height Hr is changing, tuning the height is mainly to adjust the reflection magnitude of path 2. For the vertical coupling $S_{12,4}$, the height Hr is the key parameter for suppression purposes, that is, a higher Hr results in a lower coupling level, as plotted in Fig. 3(b). However, it can be anticipated that increasing the height of the metal block

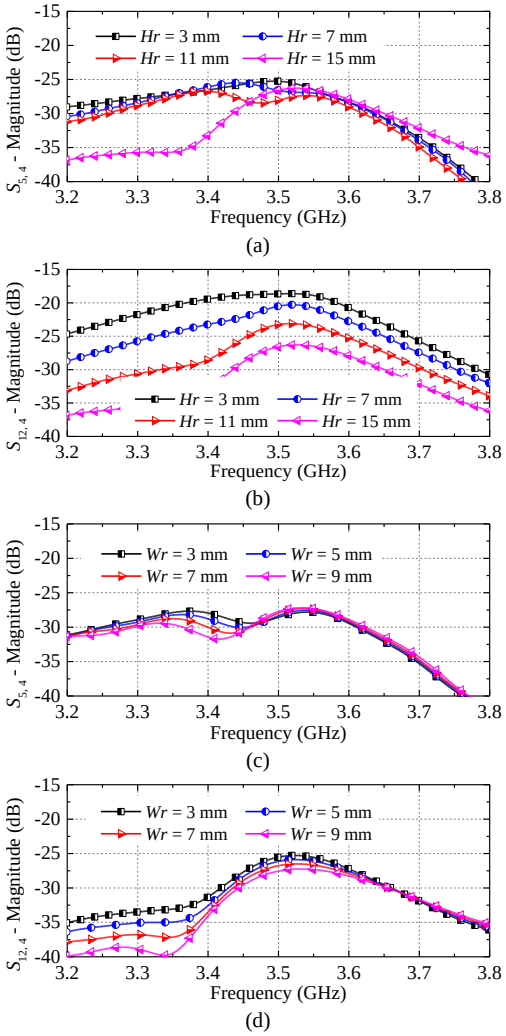

Fig. 3. Parameter studies of the mutual coupling with different dimensions of the metal block. (a) $S_{5,4}$ against Hr, where Wr = 5 mm. (b) $S_{12,4}$ against Hr, where Wr = 5 mm. (c) $S_{5,4}$ against Wr, where Hr = 14 mm. (d) $S_{12,4}$ against Wr, where Hr = 14 mm.

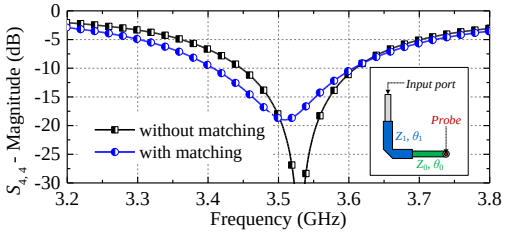

Fig. 4. Impedance matching responses with/without additional matching stubs, where Z_0 = 50 Ω, Z_1 = 40.1 Ω, θ_0 = 90°, θ_1 = 136.7°.

may lead to radiation pattern distortion since a theoretically E-wall is loaded on one side of the antenna elements. The effects of the width Wr on $S_{5,4}$ and $S_{12,4}$ are described in Fig. 3(c) and Fig. 3(d), respectively. As for $S_{5,4}$, the decoupling resonance departs away from the center frequency to lower frequencies with the width increasing. This means the changing of Wr influences both the phase and magnitude of path 2. Moreover, a wider width leads to a better decoupling level for $S_{12,4}$, but would possibly introduce radiation pattern distortion since the E-wall is closing to the elements. By following the above discussions, the physical dimensions of the decoupling metal block can be determined. Please note that there is a

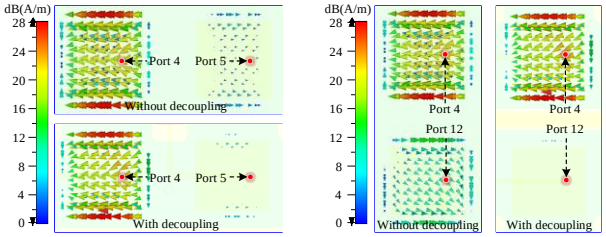

Fig. 5. Surface current distributions at 3.5 GHz with/without decoupling between (a) Port 4 and Port 5, (b) Port 4 and Port 12.

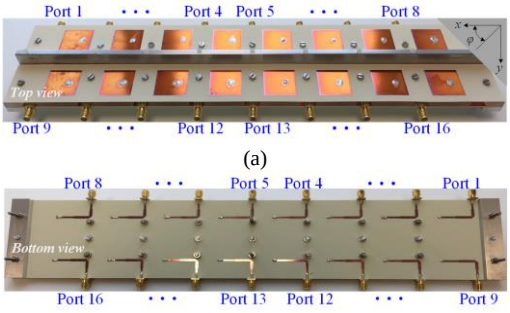

Fig. 6. Photos of the demonstrator using the proposed decoupling structure. (a) Top view, and (b) bottom view.

tradeoff between decoupling and reducing radiation pattern distortion when determining the values of *Hr* and *Wr*.

Before manufacturing the demonstrator, the impedance matching performance is also studied. Since an additional E-wall is loaded close to the antenna elements, the impedance bandwidth is slightly narrowed. To compensate for the mismatching effect, a simple two-order transformer is employed and loaded at the end of the feeding probe of every antenna element. The full-wave simulated results of the decoupled array with and without the improved matching performance are illustrated in Fig. 4, where port 4 is the representative port. It is seen that the offset of the center frequency has been amended with the help of the impedance transformer. Surface current distribution comparisons of the array with and without the proposed decoupling method are also provided, as pictured in Fig. 5. For both the horizontal and vertical pairs of the elements, the excited parasitic surface current is well-suppressed after decoupling. Next, the demonstrator will be fabricated and measured, and performance comparisons with some other published works will be given.

III. Measurement and Discussion of The Antenna

Fig. 6 illustrates the assembled demonstrator, where some metal and plastic screws are utilized for fixation purposes. The positions of the screws are fully considered during the full-wave simulations and optimized to reduce the additional effects on impedance matching and decoupling as much as possible. The array is fully tested by using the Keysight N5227A network analyzer and the in-house SATIMO SG24L spherical near-field scanner.

Fig. 7 shows the measured and simulated *S* parameters of the decoupled array, where the full-wave simulated results without decoupling are also given. The antenna elements are

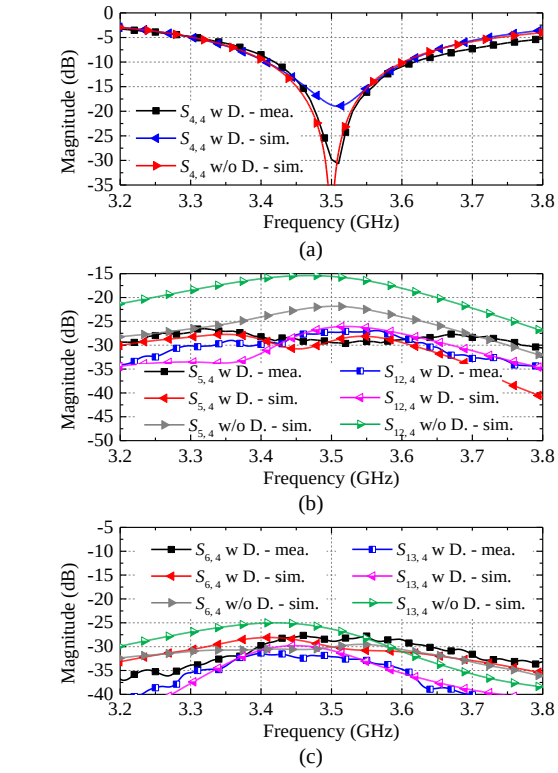

Fig. 7. Measured and simulated *S* parameters between the representative ports. (a) $S_{4,4}$. (b) $S_{5,4}$ and $S_{12,4}$. (c) $S_{6,4}$ and $S_{13,4}$.

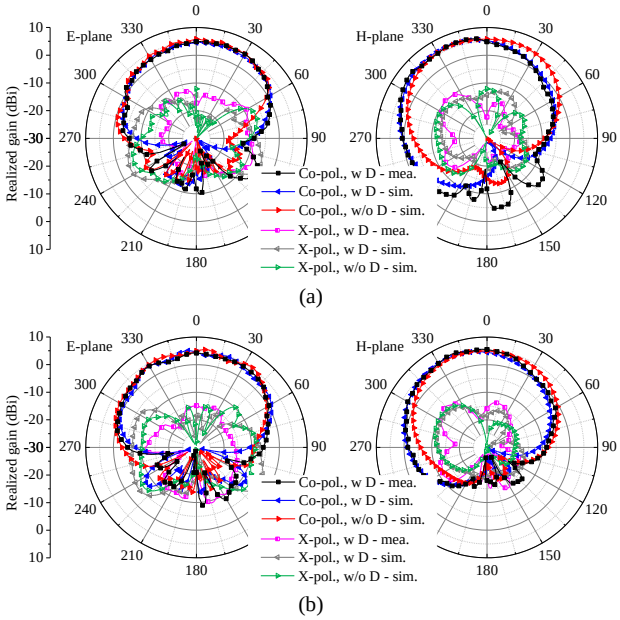

Fig. 8. Measured radiation patterns with (a) Port 1 and (b) Port 4 excited.

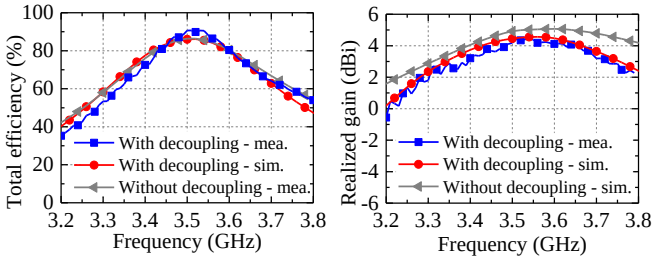

Fig. 9. Measured and simulated (a) total efficiencies and (b) realized gain at boresight direction with Port 4 excited.

TABLE I
PERFORMANCE COMPARISONS BETWEEN THE PROPOSED AND SOME PUBLISHED DECOUPLED ANTENNAS

Ref.	Array configuration	Design complexity	Profile with decoupling*	Isolation improvement	Decoupling bandwidth	Total efficiency	Insertion loss**
[14]	1×8	Complicated	$0.086\lambda_0$	10 dB	0.4%	~80%	Not given
[16]	Staggered 4×4	Complicated	$0.385\lambda_0$	14 dB	12.77%	Not given	Not given
[18]	4×4	Complicated	$0.217\lambda_0$	9 dB	2.04%	70%-82%	0.45 dB
[19]	1×8, 2×4	Simple	$0.066\lambda_0$	7 dB	4.08%	75%-80%	0.7 dB
[20]	1×4	Simple	$0.037\lambda_0$	8 dB	2.86%	Not given	Not given
This work	2×8	Very simple	$0.172\lambda_0$	11.5 dB	5.71%	> 79%	< 0.1 dB

* λ_0 denotes the free-space wavelength at the center frequency. ** denotes the additional loss introduced by the decoupling structures.

well-matched after decoupling with the impedance transformer, and the measured and simulated results are consistent with each other, as depicted in Fig. 7(a). The coupling between the horizontal elements, i.e. $S_{5,4}$, is suppressed from −21.8 dB to less than −28.1 dB within the impedance band. As for the coupling between the vertical elements $S_{12,4}$, it has been significantly reduced from −15.4 dB to less than −26.9 dB among the entire studied frequency band. The mutual coupling between non-adjacent elements is measured, as illustrated in Fig. 7(c). Particularly, the coupling between the diagonal elements, $S_{13,4}$, is suppressed from −25.1 dB to less than −31.3 dB. Other unmentioned coupling paths are still kept at a low level of less than −27 dB, which are not detailed for brevity.

The radiation patterns of the decoupled array are plotted in Fig. 8. The radiation performance at E-plane with the decoupling structure is close to the one without decoupling, while the maximum gain direction of the radiation pattern at the H-plane is slightly deflected after decoupling. The main beam slightly squints off axis in *yoz*-plane referring to the coordinate marked in Fig. 6. This is because that the decoupling metal block works as a partition device, which not only reduces the coupling between the vertical allocated elements but also breaks the structural symmetry of the radiators concerning the vertical direction. Consequently, the propagation of the electromagnetic wave would be obstructed at low elevation angles, in the area close to the block. Despite that, there is no significant difference between the performance of the array with and without the proposed decoupling structure. Moreover, considering that the decoupled antenna array operates beam scanning in *xoz*-plane, the influence of the beam squinting is limited. Fig. 9 shows the total efficiency and realized gain at the boresight direction of the array with port 4 excited. The insertion loss introduced by the decoupling block is small, and the total efficiency is higher than 79% within the impedance band. Notice that there is a discrepancy difference between the measured and simulated ones, which is mainly caused by the limited accuracy of the near-field scanner used here.

For comparison purposes, some recently published decoupling methods are summarized and listed in Table I. In [14], near-field resonators consisting of five split rings are designed where over eight parameters need to be determined and optimized. Besides, the decoupling bandwidth is narrow, which is around 0.4%. The decoupling approach provided in [16] uses specified reflecting elements to cancel the mutual coupling for large-scale arrays. The method focused on the staggered array configurations where additional phase compensation structures are essential, leading to a complicated procedure. In [18], the reported decoupling network is composed of decades of transmission lines with different characteristic impedance values and electrical lengths. These decoupling methods feature very complicated design procedures. Moreover, the total efficiency of the antenna arrays given in [18] and [19] also suffers from the additional decoupling structures, with the insertion losses of around 0.45 dB and 0.7 dB, respectively. The method studied in [20] is simple, where only the specified feeding structure of antennas needs to be modified but is effective for only E-coupled linear antenna arrays with a narrow decoupling bandwidth. As for the proposed decoupling method itself, it is very simple since only a metal block is employed. After integrating with the proposed decoupling block, the antenna array still features a compact system size and simple layout, since there is no additional surface positioned on the top of the antenna aperture [14], [16] or complicated network at the antenna feeding layer [18]. It is found that the proposed decoupling method uses a simple structure to improve the isolation by 11.5 dB. The additional insertion loss introduced by the decoupling structure is less than 0.1 dB. By simply optimizing the dimensions of the metal block, E-coupled, H-coupled as well as diagonal-coupled paths can be suppressed to a low level, with high total efficiency

IV. CONCLUSION

The strong mutual coupling among antenna elements would significantly decrease the stability of MIMO systems, especially for massive MIMO applications. To address the issue, a very simple decoupling method using a rectangular metal reflector is proposed and studied in this communication. With the presented configuration, the coupling paths at E-plane, H-plane as well as diagonal-plane are all reduced with almost no degradation on the total efficiency. A demonstrator of a 2×8 antenna array loaded with the metal block is manufactured, assembled, and tested. Both full-wave simulations and measurements verify the decoupling and radiation performance. The proposed method features a low profile and low insertion loss, and can be a potential solution for the decoupling of massive MIMO systems.

REFERENCES

[1] T. L. Marzetta, ‘‘Massive MIMO: An introduction,’’ *Bell Labs Tech. J.*, vol. 20, pp. 11-22, Mar. 2015.

[2] A. O. Martínez, J. Ø. Nielsen, E. De Carvalho, and P. Popovski, “An experimental study of massive MIMO properties in 5G scenarios,” *IEEE Trans. Antennas Propag.*, vol. 66, no. 12, pp. 7206–7215, Dec. 2018.

[3] L. Savy and M. Lesturgie, “Coupling effects in MIMO phased array,” in *2016 IEEE Radar Conference (Radar. Conf.)*, Philadelphia, PA, USA, May 2016, pp. 1–6.

[4] B. Wang, Y. Chang, and Y. Sun, “Performance of the large-scale adaptive array antennas in the presence of mutual coupling,” *IEEE Trans. Antennas Propag.*, vol. 64, no. 6, pp. 2236-2245, Jun. 2016.

[5] H. Makimura, K. Nishimoto, T. Yanagi, T. Fukasawa, and H. Miyashita, “Novel decoupling concept for strongly coupled frequency-dependent antenna arrays,” *IEEE Trans. Antennas Propag.*, vol. 65, no. 10, pp. 5147–5154, Oct. 2017.

[6] E. Rajo-Iglesias, Ó. Quevedo-Teruel, and L. Inclán-Sánchez, “Mutual coupling reduction in patch antenna arrays by using a planar EBG structure and a multilayer dielectric substrate,” *IEEE Trans. Antennas Propag.*, vol. 56, no. 6, pp. 1648–1655, Jun. 2008.

[7] S.-W. Su, C.-T. Lee, and Y.-W. Hsiao, “Compact two-inverted F-antenna system with highly integrated π-shaped decoupling structure,” *IEEE Trans. Antennas Propag.*, vol. 67, no. 9, pp. 6182–6186, Sep. 2019.

[8] L. Zhao, and K.-L. Wu, “A decoupling technique for four-element symmetric arrays with reactively loaded dummy elements,” *IEEE Trans. Antennas Propag.*, vol. 62, no. 8, pp. 4416–4421, Aug. 2014.

[9] F. Liu, J. Guo, L. Zhao, G.-L. Huang, Y. Li, and Y. Yin, “Dual-band metasurface-based decoupling method for two closely packed dual-band antennas,” *IEEE Trans. Antennas Propag.*, vol. 68, no. 1, pp. 552–557, Jan. 2020.

[10] D. Gao, Z.-X. Gao, S.-D. Fu, X. Quan, and P. Chen, “A novel slot-array defected ground structure for decoupling microstrip antenna array,” *IEEE Trans. Antennas Propag.*, 2020. DOI: 10.1109/TAP.2020.2992881

[11] X. Yu, and H. Xin, “Direction-of-arrival estimation enhancement for closely spaced electrically small antenna array,” *IEEE Trans. Microw. Theory Tech.*, vol. 66, no. 1, pp. 477-484, Jan. 2018.

[12] J. Sui and K.-L. Wu, “Self-curing decoupling technique for two inverted-F antennas with capacitive loads,” *IEEE Trans. Antennas Propag.*, vol. 66, no. 3, pp. 1093-1101, Mar. 2018.

[13] Y. M. Pan, X. Qin, Y. X. Sun and S. Y. Zheng, “A simple decoupling method for 5G millimeter wave MIMO dielectric resonator antennas,” *IEEE Trans. Antennas Propag.*, vol. 67, no. 4, pp. 2224-2234, Apr. 2019.

[14] M. Li, B. G. Zhong, and S. W. Cheung, “Isolation enhancement for MIMO patch antennas using near-filed resonators as coupling-mode transducers,” *IEEE Trans. Antennas Propag.*, vol. 67, no. 2, pp. 755-764, Feb. 2019.

[15] K.-L. Wu, C. Wei, X. Mei, and Z.-Y. Zhang, “Array-antenna decoupling surface,” *IEEE Trans. Antennas Propag.*, vol. 65, no. 12, pp. 6728-6738, Dec. 2017.

[16] C. Wei, Z.-Y. Zhang, and K.-L. Wu, “Phase compensation for decoupling of large-scale staggered dual-polarized dipole array antennas,” *IEEE Trans. Antennas Propag.*, vol. 68, no. 4, pp. 2822-2831, Apr. 2020.

[17] R.-L. Xia, S.-W. Qu, P.-Fa Li, D.-Q. Yang, S. Yang, and Z.-P. Nie, “Wide-angle scanning phased array using an efficient decoupling network,” *IEEE Trans. Antennas Propag.*, vol. 63, no. 11, pp. 5161-5165, Nov. 2015.

[18] Y.-M. Zhang, S. Zhang, J.-L. Li, and G. F. Pedersen, “A transmission-line-based decoupling method for MIMO antenna arrays,” *IEEE Trans. Antennas Propag.*, vol. 67, no. 5, pp. 3117-3131, May 2019.

[19] Y.-M. Zhang, S. Zhang, J.-L. Li, and G. F. Pedersen, “A wavetrap-based decoupling technique for 45°-polarized MIMO antenna arrays,” *IEEE Trans. Antennas Propag.*, vol. 68, no. 3, pp. 2148-2157, Mar. 2020.

[20] H. Lin, Q. Chen, Y. Ji, X. Yang, J. Wang, and L. Ge, “Weak-field-based self-decoupling patch antennas,” *IEEE Trans. Antennas Propag.*, vol. 68, no. 6, pp. 4208-4217, Jun. 2020.